International Journal of Thermophysics (2023) 44:63
https://doi.org/10.1007/s10765-023-03165-7

Characteristics of Viscosity of a Scale Inhibitor: An Experimental Study

Sindre Kalstad Gamst[1] · Espen Fanøy Salo[1] · Eirik Smith Eide[1] · Habtamu Bayera Madessa[1] · Arnab Chaudhuri[1]

Received: 28 November 2022 / Accepted: 31 January 2023 / Published online: 6 March 2023

Abstract

The use of chemical scale inhibitors in the oil and gas industry for subsea installations has been presented for a long time, but the ever-increasing exploration of HPHT (high pressure high temperature) wells put demands on knowledge of how the rheological properties such as viscosity of scale inhibitors behave under large pressures. This work reports new experimental data of high-pressure viscosity using a rotational rheometer, measured across a pressure range of 0.1 MPa to 15 MPa, at temperatures from 273 K to 298 K, and a broad range of shear rates, 100 s^{-1} to 1000 s^{-1} for a scale inhibitor. The experimental data are used to construct a power-law regression model with fitting parameters. Results indicate that the inhibitor shows a near Newtonian behavior.

Keywords High-pressure viscosity · Oilfield Scale inhibitor · Regression analysis · Rheological experiments

✉ Arnab Chaudhuri
arnab.chaudhuri@oslomet.no

Sindre Kalstad Gamst
mr.sindre@yahoo.no

Espen Fanøy Salo
salo.espen@gmail.com

Eirik Smith Eide
eirik.eidesmith@gmail.com

Habtamu Bayera Madessa
habama@oslomet.no

[1] Department of Civil Engineering and Energy Technology, OsloMet – Oslo Metropolitan University, Pilestredet 35 PB 4 St. Olavs plass, Oslo 0130, Norway

1 Introduction

In an oil and gas subsea extraction process, one simultaneously extracts reservoir formation water from the well and seawater from the surroundings, both of which contain saturated minerals of different kinds. These minerals have been maintained at equilibrium for millions of years, but contact with seawater and changes to their intensive properties, such as temperature and pressure, might cause modifications to the minerals. This lays the foundation for potential precipitation deposits. These deposits (the scaling) build up as crystalline structures inside the production pipe and restrict the production flow, potentially blocking the pipe all together. If nothing is done to inhibit the buildup of scale, then the production well will eventually stop to a complete halt, a process seen to happen in as short as 24 h [1] This can be a costly affair as the price tag for the removal of scale in a single well can be as much as 2.5 million dollars [2].

There are several techniques to deal with scale formation, from scale removals to scale inhibition. Due to the potential disastrous consequences of scaling, there is widespread production and design of scale inhibitors (SIs), all with the goal of efficient scale inhibition. As these chemicals are transported through pipes of long distances and operating under pressures up to 17 MPa, the rheological qualities of the chemicals are important. How they react to the subsea temperatures, the velocity of which they are being transported at, and the high pressure they are being subjected to are crucial. Consequently, an increase of viscosity in mid-transportation can cause fluid flow to decrease, resulting in similar problems caused by scale. In this context, the motivation of the present study is to investigate and test a scale inhibitor under high pressure and varying shear rates, studying the relationship between the chemical's viscosity and pressure, shear rate, and temperature. After reviewing the existing literature, not much material has been found on the research done related to the rheological properties of scale inhibitors. However, we provide an account of scientific endeavors related to the general viscosity measurements at high pressure, looking at existing work done for fluids like biodiesels, biofuels, synthetic oils, and heavy/crude oil. The pressures measured in these studies are also higher than that of the experiment carried out for this work.

1.1 Effects of High Pressure

As the search for oil progresses in more and more hostile environments, at high temperature and high pressure (HTHP), the window for oil drilling decreases, risk of increased corrosion, and there's a need for more specialized equipment. To increase stability in pumping and transportation of oil, close supervision of the parameters in the pipes is necessary. Installing viscometers and sensors is not only costly, but also difficult to operate. Therefore, accurate models can function as a great alternative [3]. Processes such as flat-rolling of steel, with pressures up to 500 MPa andabove, are common [4, 5]. The viscosity of a lubricant is directly related to the resistance of flow, which, in the case of lubricants, is linked to its utility as a lubricant. How

it changes under large pressure has therefore been an important area of study for a long time, and numerous equations has subsequently been developed.

Several studies of viscosity changes due to high pressure exist. These are predominantly focused on the pressure and temperature range of 0 MPa to 150 MPa and around 290 K to 390 K. The majority of these are experimental works, and the use of a falling ball/sinker viscometer is dominant. The common way of calculating the viscosity for this instrument is by the use of an equation introduced in a PhD dissertation by Vant [6] (2003), which takes into account density of the falling object and the sample liquid, as well as the fall time. An upside of the use of such an instrument is shown to be the reproducible, as well as the possibility of measuring fall time at extreme pressures, with examples as high as 20,000 MPa [7]. The downside is, however, the need to determine the accurate correction factors based on densities of the liquid and falling object, limiting values of shear rate, together with the need to precisely track the position of the object [8]. The use of falling ball/sinker viscometers relies heavily on the use of theoretical models to compute viscosity. Others have done similar experiments using different instruments. Rotational and vibrating wire viscometers have been used, which allows for a wider range of parameters in the experiments. One such parameter is the shear rate. The shear rate ranges vary widely, from 10–200 s^{-1} to 10–1000 s^{-1}. In their study [9], the authors reported that a type of synthetic oil actually showed Newtonian behavior at shear rates below 600 s^{-1}, while it behaved as a non-Newtonian fluid at higher shear rates. Results for existing literature reveal a clear tendency for viscosity to grow exponentially with pressure, while viscosity decreases with an increase of temperature. The study by Sobrino et al. [10] measured pressure at 0 MPa to 120 MPa, Freitas et al. [11] went from 0 to 1400 bar, which is the same as Lineira et al. [9]. Viscosity often sees rather modest changes in the pressure range from 0.1 MPa to 30 MPa [12]. These results cited here are well above this, and often, it is beyond ≈30 MPa that any exponential trend starts. Given that the behavior of the viscosity is exponential as pressure increases, many have also tried to fit experimental data to a numerical model, with the goal of it being predictive for future applications. These have often shown to be modifications of the Barus equation, originally presented in 1893 [13] as $\eta_P(T,P) = \eta_0(T)e^{\alpha P}$ with T and P being temperature and pressure, while η_0 is the dynamic viscosity at atmospheric pressure, and α is the pressure viscosity coefficient (PVC) and can be viewed as the slope if one plots viscosity vs pressure. Another way of representing the Barus equation is by adding atmospheric pressure, 0.1 MPa, in the exponent as $\eta_P(T,P) = \eta_0(T)e^{\alpha(P-P_o)}$. While Barus is rather limited to lower pressures, Freitas et. al [11] has made a model valid for high pressures with $\ln\eta = \ln\eta_o + a\frac{P-P_0}{T^b}$, where η_0 is the viscosity measured at P_0=0.1 Pa. $a = 1.2$ and $b = 0.84$. Table 1 summarizes the experimental values for different liquids, their predictive model equation, based on either Barus or Freitas coefficients, PVC values, and R^2 values, with general temperature and pressure ranges of 283 K to 373 K & 0.1 MPa to 140 MPa. The substances with PVC values denoted as “PVC" are taken from an elaborate table by Ferreira et. al [14]. r^2 is the *coefficient of determination* (measure regression model performance).

The use of the Barus equation and some clever modification for high-pressure scenarios seems to be the normal starting point in constructing a model that fits

Table 1 Model equations, coefficients, PVC, and coefficient of determination for different substances

Substance	Model equation	η_0	PVC/coefficients	R^2
Substances in table 11 in [14], P[MPa]	$\eta_P(P) = \eta_0 e^{\alpha(P-P_o)}$			
Rapeseed [11]		$\eta_0 = 6.93$	PVC = 0.01327	
Combined mixture [11]		$\eta_0 = 6.760$	PVC = 0.01172	0.999
Soybean [16]		$\eta_0 = 7.416$	PVC = 0.01141	0.998
Coconut [16]		$\eta_0 = 4.857$	PVC = 0.01054	0.997
Canola [16]		$\eta_0 = 8.569$	PVC = 0.01155	0.999
Usedcanola [16]		$\eta_0 = 8.615$	PVC = 0.01138	0.999
Jatropha Oil [16]		$\eta_0 = 8.54$	PVC = 0.01212	1.000
Vistive Oil [16]		$\eta_0 = 7.767$	PVC = 0.01121	0.998
Soybean [11]	$\ln \eta = \ln \eta_0 + \alpha(\frac{P-P_0}{T^\beta})$		$\alpha = 1.2, \beta = 0.86$	
T[K], P[MPa], η[mPas]				
Ionic liquids [15], T[K]:				
([PF_6])	$\eta = \eta_0 e^{\frac{B}{T-T_0}}$	$\eta_0 = 1.06$	B = 10.0, T_0=1.71	
([BF_4])		$\eta_0 = 0.89$	B = 9.37, $T_0 = 1.64$	
Vegetable oil [17],P[MPa]	$\eta_P(P) = \eta_0 e^{\frac{P}{\beta}}$	$\eta_0 = 89.648$	$\beta = 76.923$	
Biodiesel (WCO) [18]		$\eta_0 = 9.728$	$\beta = 84.74$	0.988
Rapeseed [18]		$\eta_0 = 7.557,$	$\beta = 89.28$	0.996
Diesel A [18]		$\eta_0 = 3.311,$	$\beta = 75.53$	
Diesel B [18]		$\eta_0 = 3.567,$	$\beta = 76.33$	
Diesel C [18]		$\eta_0 = 2.474,$	$\beta = 74.63$	

The uncertainties of viscosity measurements are as follows: in Ref. [11] it is 1% , in Ref. [14] it varies between 0.2% to 3 %, and in Ref. [15] it is ±2.1%. The uncertainty for viscosity is not reported in Refs. [16–18]

empirical data. But other equations such as the Hybrid model and the Roeland equation are also commonly used. These equations also take into account the variable of temperature as $\eta(T,P) = \eta_0 \left(\frac{\eta_\infty}{\eta_0}\right)^{(1-(1+P/r)^z)}$, where η_0 = Dynamic viscosity at ambient pressure [Pa.S], $\eta_\infty = 6.315\times10^{-5}$ [Pa.s], $r = 1.96\times10^8$ [Pa], P = Pressure [Pa] z = Pressure-viscosity coefficient [-]. However, predictions from Barus and Roeland equations often differ significantly. Also, Barus equation tend to produce erroneous results at high pressure [19] (a factor upto 500). This error is of such a magnitude that some has advised against its use on pressures larger than 500 MPa [20]. It has also been shown that the Barus equation can give even worse predictions at elevated temperatures [21]. For most of the modifications of the Barus equation and other similar equations, the emphasis has been on constructing a fitting PVC, with the PVC being the exponent in the Barus equation. The coefficient can be derived by plotting the viscosity on a logarithmic scale versus pressure. This has been done to numerous lubricants, and based on these data, several attempts to construct a general analytic formulae for obtaining the coefficient have been tried, where among them, the formula obtained by So and

Klaus (see Equation 1) is regarded as one of the best [21, 22]. The α value is another way to denominate pressure–viscosity coefficients.

$$\begin{aligned}\alpha =& 1.216 + 4.143(\log \mu_0)^{3.0627} + 2.848 \times 10^{-4} m_0^{5.1903} (\log \mu_0)^{1.5976} \\ & - 3.999(\log \mu_0)^{3.0975} \rho^{0.1162}\end{aligned} \tag{1}$$

where μ_0 kinematic viscosity of the fluid at atmospheric pressure, ρ being the density at atmospheric pressure, and m_0 a viscosity–temperature property. This property stems from a chart by ASTM (American Society for Testing Materials) and is based on empirical data. Much like the PVC (or α coefficient) being the slope of a viscosity–pressure graph, this m_0 property can be viewed as the slope of a viscosity–temperature graph [21]. On a microscopic level, the coefficient is said to be a function of several physical characteristics of the fluid such as molecular interlocking, packing, rigidity, and temperature. However, it can also be independent of both temperature and pressure, such as the Roeland equation [21]. The coefficient has therefore been reported to hold different values for different fluids at different temperatures [21].

1.2 The Effect of Shear Rate

Although not mentioned in the section and formulas above, the effect that shear rate has on the viscosity of certain liquids is well established. br>In tribology-related lubricants, there are examples of large shear rates having a direct impact on the accuracy of the estimation of viscosity [21]. On the other hand, the literature regarding “low initial viscosity liquids," can be regarded as sparse. All of these different liquids will react substantially different from each other to the applied level of shear rate. Due to this diversity of non-Newtonian rheological behavior, a single formula that predicts this has not yet been achieved. Attempts have been made to combine the empirical and theoretical approaches yielding models that are dependent on non-Newtonian behavior [23]. In the literature of non-Newtonian fluids, there is established a category of fluids named *generalized non-Newtonian fluids* for which the non-Newtonian viscosity is a function of the shear rate and is also time independent. There are a few common semi-empirical models used to fit data and a further discussion of them will follow. The first equation is known as a simple equation for modeling non-Newtonian fluids and regarded as the most used model in process-related engineering [23]. It is a type of power-law and often goes by the name Ostwald-de Waele equation: where κ is known as the consistency coefficient and n is a power-law index, both of which are empirical curve-fitting parameters. The value of n indicates the non-Newtonian behavior where ($n < 1$) indicates shear-thinning behavior, ($n = 1$) indicates classical Newtonian behavior, and ($n > 1$) indicates shear-thickening behavior. The power-law model is, as stated above, a simple model and therefore has some obvious downsides due to its simplicity. For the most part, it only gives approximations and is mostly just valid for a limited range of varying shear rates, which means that the values for n and κ are dependent on a chosen shearing range [23]. Since every non-Newtonian liquid is unique in its behavior, deviation from empirically based models should be expected, and better models with more fitting parameters have therefore been developed. These models have often been a response

to values of viscosity approximating Newtonian behavior at high and/or at low shear rates.

It is important to mention that in the section above regarding how high pressure affects viscosity, there were a few studies that reported how viscosity changes with increasing pressure, at a given shear rate between 100 s^{-1} and 1000 s^{-1} [9–11]. These results still showed a clear tendency for exponential increase in viscosity due to pressure regardless of the value of shear rate. As high-pressure analysis of fluids becomes increasingly important in a wide range of industries, from food processing, fluid injection in combustion engines, to the oil and gas industry, the fluids analyzed vary equally. Many of the articles referenced here have used diesel fuels, or biofuels/oils [11, 17, 18], while others focus on heavy crude oil [24], synthetic oils [9], and oil-based drilling fluids [25].

This work focuses, however, on scale inhibitors, and the analysis of inhibitors in general is lacking in the literature. In the efforts of making the above literature review, it has become clear that the piezoviscous effects of any fluids is not a prioritized field of research, though there have been conducted extensive research in the field of tribology along with the oil and gas industry on rheological properties in high-temperature conditions. In contrast to this, the effect of pressure on viscosity, even for simpler Newtonian fluids, is still largely a mystery and the research is in its infancy [8]. The rest of the article is organized as follows. We briefly present the experimental setup in Sect. 2, followed by results and discussions in Sect. 3. Finally, the conclusions are drawn in Sect. 4.

2 Method

The material tested in this work is a scale inhibitor produced by Clariant AG and provided by Aker Solutions, Norway. A detailed composition of the chemical and further specifications is not provided as they remain classified. From what is known of the chemical liquid tested is that it's ethanediol-based. These types of inhibitors are named Thermodynamic Hydrate Inhibitors (THIs) and have usually been used to prevent the risk of hydrate causing problems in piping, where they shift the thermodynamic conditions at where hydrate forms. THIs are a robust choice for long distance oil and gas tie-backs, as they work well in the lower temperatures and high pressures. Now with new and improved chemical compositions they're also used to prevent the buildup of scale in the oil and gas industry [26].Colloquially referred to as ethylene glycol or monoethyleneglycol (MEG), which are mostly used as antifreeze to lower the freezing point of coolants in cars or in buildings. MEG is also in use as solvents in paint and plastic industry [27].

The rotational rheometer is today regarded as one of the most common instruments used in rheological experiments. It is regarded as a highly accurate instrument and easily programmable. Since it is driven by a motor, it is open for investigating a wider range of viscous liquids than compared with the other viscometers. A good starting point to get an idea of the workings of this instrument is to look at the two-plate model and imagining bending the two plates into two concentric cylinders. The gap between the cylinders can then be filled with the sample and a rotational velocity

of the inner cylinder can be initiated by a given torque from the motor, while the outer cylinder is fixed. The sample can then be put into laminar flow, and values for shear rate, shear stress, and viscosity can be mathematically extracted from gathered data and on the chosen measuring program. The inner cylinder is referred to as a bob. The rotational parts of the rheometer do not need to be concentric cylinders. Other types are double gap geometries, cone-plate measuring systems, etc. For this work, a double gap cylinder was used. The advantage of such a solution is the low risk of turbulence to occur, while simultaneously being able to test low viscosity liquids. One main feature of the double gap is the increased shear area. As the cylinder being used is hollow, both the inside and outside of the cylinder are in contact with the sample, thus doubling the effective shear area [12]. This allows to measure at lower shear rates than would be possible with a concentric cylinder geometry.

The viscometer used for the experiment is a rotational rheometer from Anton Paar, more specifically an *Anton Paar MCR 301*. Additionally, a pressurized cell was used to reach pressures of 15 MPa, with nitrogen being the pressurized gas. The instrument included a double gap geometry, with magnetic coupling to induce torque on the bob. In this experiment, the bob was a coaxial cylinder bob setup with double gap geometry, an Anton Paar DG23 with external and internal cup diameter of 23.85 mm and 20.33 mm. The external and internal diameters of the coaxial cylinder bob are 23.04 mmand 21.03 mm. The accuracy for the torque is said to be max. 0.2 μNm, or 0.5%, with a resolution of 0.001 μNm for the MCR 301, while the temperature channel of the instrument has an accuracy of $\pm$0.03 K, with a resolution of 0.01 K. The instrument was supplied by the Colloid, Interfacial, and Fluid Research Laboratory (CIRLAB) at the Institute for Energy Technology (IFE), and the experiments were executed at their lab during two consecutive days. Figure 1 shows the instrument and the double gap geometry for the bob.

2.1 Procedure

A calibration procedure initiated the experiment, using a standard 135 calibration oil provided by Anton Paar, with a viscosity of 135 mPa.s. The readings from the instrument were then compared with a table of known values. The viscosity of the scale inhibitor was measured under different conditions of temperature, pressure, and shear rate, as indicated in Table 2.

The viscosity measurements were performed using manual injection. Nitrogen gas was used to get the desired pressures for the measurements. The protocol for the measurements is provided below:

1. The oil sample was introduced into the pressure cell of the rheometer (manual injection).
2. The geometry was inserted into the sample.
3. The sample was pressured by nitrogen for desired pressure values (from ambient to 15 MPa)
4. The measurement was started.

(a) Anton Paar MCR 301 Rheometer with the connected nitrogen tank used for running the experiment

(b) High pressure set up in Double Gap geometry

Fig. 1 Instrument (a) is located in the Colloid, Interface, and Fluid Research Laboratory (CIRLAB) at IFE, Kjeller and (b) was taken from the Anton Paar website [28]

Table 2 The range of conditions of the test

Variables	Values
Pressure (MPa)	0.1–15
Temperature (K)	0–298
Shear rate (s^{-1})	100–1000

Each sample was pre-mixed for 5 min for each temperature at a shear rate of 100 s^{-1} before the measurements started. The sample size used each time was $\approx$ 5 mL. As the pressure needed to be adjusted manually after each sample was injected, this would need to be kept constant for each measurement. The measurements themselves consisted of several “sweeps"; after the sample was injected and pressurized, the instrument would start running at a temperature of 273 K and a shear rate of 100 s^{-1}. Then, while keeping the temperature constant, the shear rate would increase from 100 s^{-1} to 1000 s^{-1}, recording data using 30 measurement points over a 5-s period. After the shear rate reached 1000 s^{-1}, it would lower it to 100 s^{-1} again, before increasing the temperature to 278 K and repeating the process. This was done for temperatures of 273 K, 278 K, 283 K, 288 K, 293 K, and 298 K for 8 different

pressures in the range of 0.1–15 MPa. It is important to bring to light some limitations of the instrument which could lead to faulty readings and illogical results. According to professionals at IFE, there is a weakness of the double gap geometry for lower shear rates, especially below $\approx 200\ s^{-1}$. This has shown to be the case for several other experiments conducted using the same instrument and geometry. Another choice of geometry might yield sufficient results also at lower shear rates, but as this experiment was conducted in a high-pressure chamber, the double gap geometry with magnets was chosen. As mentioned earlier, a calibration fluid was used beforehand to check the instrument, which showed that this weakness does not affect measurements at shear rates above $200\ s^{-1}$. On the account of this, the results presented in Sect. 3 will include datasets at minimum $300\ s^{-1}$ to fully reduce the risk of including misleading data, also in the event that this weakness affects the sample just above $200\ s^{-1}$.

3 Results and Discussions

In Sects. 3.1 and 3.2, we first present the raw experimental data to illustrate the characteristics of the viscosity variation with pressure and shear rate for different temperatures as mentioned in Table 2. The regression analysis is then performed to develop a power-law relation from the data and discussed in Section 3.3.

3.1 Viscosity vs Pressure

Figures 2a and b show the variation of viscosity with pressure for two different values shear rates $300\ s^{-1}$ and $1000\ s^{-1}$ while the temperature varies from 273 K to 298 K.

It can be seen that there is a tendency for the viscosity to increase marginally with pressure. while viscosity monotonically increases with decreasing temperatures. Note that at $300\ s^{-1}$, the increase of viscosity is ≈ 6.0 mPa.s when pressure increases from 0.1 MPa to 15 MPa. For lower shear rate, the maximum value of

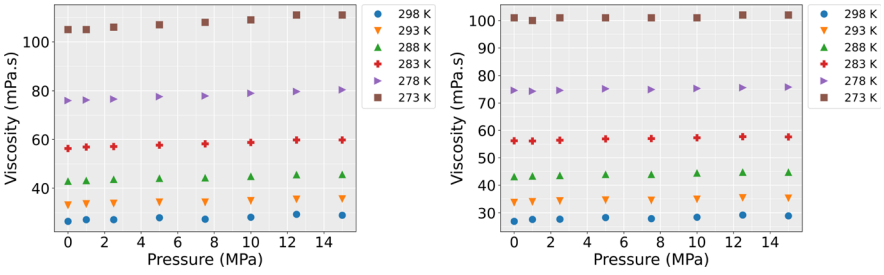

(a) *viscosity vs pressure with varying temperatures at shear rate* $300\ s^{-1}$ (b) *viscosity vs pressure with varying temperatures at shear rate* $1000\ s^{-1}$

Fig. 2 Variation of viscosity with pressure for the different temperatures at two different shear rates

viscosity at 298 K is ≈ 29.0 mPa.s, while at 273 K, it is about 82.0 mPa.s higher (almost four times). At 1000 s^{-1} (see Fig. 2b), we observe the maximum viscosity of ≈ 29.2 mPa.s at 298 K. On the other hand, the maximum is about 102 mPa.s at 273 K, which is a difference of 72.8 mPa.s. It is interesting to look into the viscosity in terms of $\Delta\mu_i = \mu_i - \mu_{start}$, which is the difference between the viscosity at different pressures and the initial viscosity. Here, μ_i is the viscosity at a pressure and a constant temperature, and μ_{start} is the first data point at that temperature. These delta values are shown in Fig. 3

What becomes evident from Fig. 3a and b is that at lower shear rates, the delta values are higher. This means that the viscosity increases more with pressure at lower shear rates than higher. For example, at 278 K and 300 s^{-1} , the viscosity has increased ≈ 4.4 mPa.s from 0.1 MPa to 15 MPa, while at the same temperature and 1000 s^{-1} ,the viscosity undergoes an increase of only ≈ 1.2 mPa.s. Another point to be made is that according to Fig. 3a, the viscosity increases more for lower temperatures at 300 s^{-1}, with an increase of ≈ 2.5 mPa.s at 298 K and ≈6.0 mPa.s at 273 K. On the other hand, at 1000 s^{-1} , viscosity increases more for higher temperature (see Fig. 3b). At this shear rate, there is an increase of ≈ 2.0 mPa.s at 298 K, and ≈ 1.0 mPa.s at 273 K. It also shows that the viscosity tends to grow substantially less at higher shear rates. At 300 s^{-1} and 278 K, which showed $\Delta\mu$ ≈4.4 mPa.s at 15 MPa, this is an increase of roughly 6 %. The viscosity at the same temperature and pressure at 1000 s^{-1} increase only about 1.6 %. A similar trend is observed at higher temperatures as well. At 298 K and 300 s^{-1} , there is an increase of ≈ 9%, while at 1000 s^{-1} , the increase is ≈ 7%. By looking at the results presented above, one can assume that temperature is the input variable with the largest effect on viscosity, while the effect of both shear rate and pressure on the viscosity is of lesser extent.

3.2 Viscosity vs Shear Rate

Figure 4a and b shows the variation of viscosity with shear rates for two different values of pressures 0.1–15 MPa while the temperature varies from 273 K to 298 K.

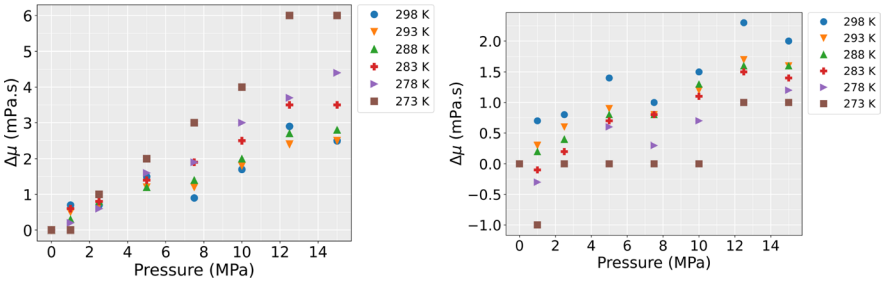

(a) $\Delta\mu$ *(mPa.s) vs pressure with varying temperatures at shear rate 300* s^{-1}

(b) $\Delta\mu$ *(mPa.s) vs pressure with varying temperatures at shear rate 1000* s^{-1}

Fig. 3 Variation of $\Delta\mu$ with pressure for the different temperatures and two different shear rates

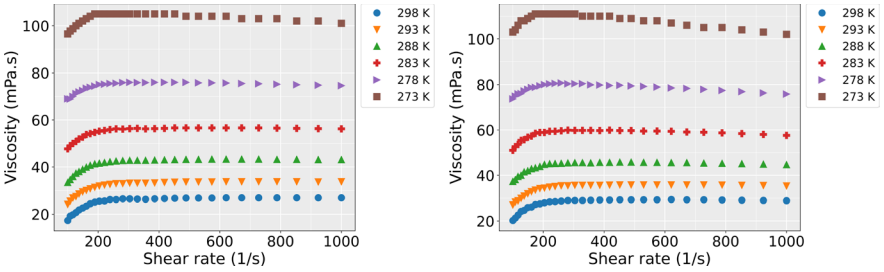

(a) *Viscosity vs shear rate for different temperatures at 0.1 MPa* (b) *Viscosity vs shear rate for different temperatures at 15 MPa*

Fig. 4 Variation of viscosity with shear rate for different temperatures at two different pressures

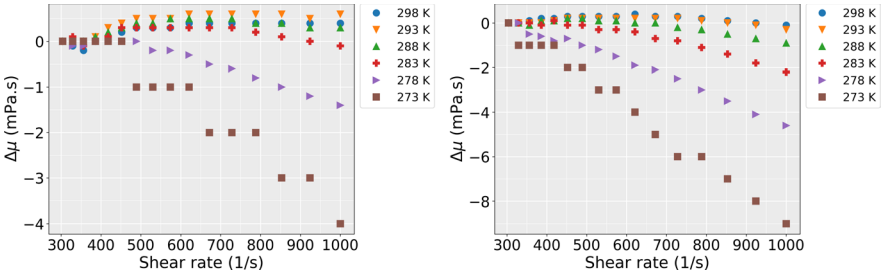

(a) $\Delta\mu$ *(mPa.s) vs Shear rate at 0.1 MPa* (b) $\Delta\mu$ *(mPa.s) vs Shear rate at 15 MPa*

Fig. 5 Variation of $\Delta\mu$ (mPa·s) with shear rate for two different pressures

The isotherms for both figures behave similar to that depicted in Fig. 2. The predominant inverse relationship between viscosity and temperature is evident from these figures.

What is interesting to notice from these figures is that the viscosity seems to show a smooth moderate increase when the shear rate grows from 100 s^{-1} to about 200–250 s^{-1}. In Fig. 4a, the viscosity flattens out and remains fairly constant all the way up to 1000 s^{-1} for all temperatures. On the other hand, Fig. 4b shows that viscosity starts decreasing past this point. Looking at the graphs, this decline is most noteworthy for lower temperatures, especially at 273 K. At higher temperatures, the viscosity does not change much with shear rate past 200–250 s^{-1}. $\Delta\mu$ values have been calculated similar to that reported in Sect. 3.1. Here, $\Delta\mu$ (Fig. 5) indicates $\mu_i - \mu_{start}$, where μ_i is the viscosity at certain viscosity and temperature, and μ_{start} is the reference viscosity, at 300 s^{-1} and at the same temperature. μ_{start} was chosen to be 300 s^{-1} and not 100 s^{-1} for reasons mentioned in Sect. 2.1.

These figures show a very similar behavior at the two pressures. At 0.1 MPa, there is a steep decrease in $\Delta\mu$ at 273 K and 278 K, while at the rest of the temperatures, the viscosity does not undergo large changes. For example, at 278 K, one could notice that there is a total decrease of ≈1.4 mPa.s, which is about 1.8 % decrease for shear rate from 300 s^{-1} to 1000 s^{-1}. At 273 K, this decrease is calculated to be 4.0 mPa.s, a fall of ≈3.8 %. At higher temperatures, this change is practically

negligible, e.g., at 283 K, the viscosity drops only by 0.1 mPa.s (or ≈0.2 %). At the maximum temperature of this experiment, 298 K, the viscosity rather increases by ≈0.4 mPa.s. It can be seen that at higher pressure (15 MPa), viscosity decreases for all temperatures. At 273 K, the viscosity drops roughly 9.0 mPa.s, while it is ≈ 4.6 mPa.s at 278 K. This represents a percentage change of ≈5.7 %. The smallest drop in viscosity occurs at 298 K at only 0.1 mPa.s. Even though the figures show a decrease at higher pressures, the $\Delta\mu$ values are not significant for temperatures greater than 283 K.

3.3 Regression Analysis

Here, we attempt to find a power-law of the form $\mu(T, P, \dot{\gamma}) = A\, T^a\, e^{bP}\, \dot{\gamma}^c$. In order to formulate the power equation, one needs to use the logarithmic values of viscosity, temperature, and shear rate. This will result in the following equation: $log\, \mu = log\, A + a\, log\, T + b\, P + c\, log\, \dot{\gamma}$. A linear regression can thus be performed based on the three parameters used in the experiment with this log transformation.

Before initiating the analysis itself, all parameters are non-dimensionalized by a suitable *reference state*, which is chosen to be 452 s^{-1} for the shear rate $\dot{\gamma}_{ref}$, which is the middle value in the interval measured at, from 100 s^{-1} to 1000 s^{-1}. The data used, however, do not include data for viscosity below 300 s^{-1}. For pressure, P_{ref} ,it is chosen to be 7.5 MPa, again the middle value, while temperature, T_{ref} , is 278 K, the realistic temperature on the seabed. The reference value for viscosity, μ_{ref} , is chosen to be 77.6 mPa.s, which is the measured viscosity at P_{ref}, T_{ref} , and $\dot{\gamma}_{ref}$. The basis of the choice of these values as reference state is explained in this section after the regression equation. Thus, the non-dimensional parameters are given by:

$$\dot{\gamma}^* = \frac{\dot{\gamma}}{\dot{\gamma}_{ref}} \quad T^* = \frac{T}{T_{ref}} \quad P^* = \frac{P - P_{ref}}{P_{ref}} \quad \mu^* = \frac{\mu}{\mu_{ref}}$$

This will result in the power-law equation with non-dimensional parameters as follows:

$$\mu^*(T^*, P^*, \dot{\gamma}^*) = A\, T^{*a}\, e^{bP^*}\, \dot{\gamma}^{*c}.$$

The performance of the model fit can be seen by the *coefficient of determination*, R^2. In the equations above, there are a different number of terms, some constant coefficients and some inputs. Each input has its own weighted coefficient, and with each coefficient, a *standard error* follows. This is a measure of the standard deviation for the error in measuring the coefficient. A large number indicates a large standard deviation, which in turn means a less accurate coefficient. In other words, the standard error for the coefficients showcases how confident the model is of the weighted coefficient. One issue that may spawn for multi-variable analysis is *multicollinearity*, the concept that input variables show some correlation among them. This may negatively affect the regression predictions and lower the statistical significance of the weighted coefficients. The results when all variables are present might not be affected as much, while the one-to-one

dependency of the predictor–input relationship might have less validity. One way to check for these multicollinearity problems is by looking at the *variance inflation factor*, VIF, that shows the level of multicollinearity for a set of variables. This is a factor, at minimum 1, that shows the correlation for each predictor. A value of 1 indicates zero multicollinearity for that predictor, while a value of 10 or more indicates that some correction to the dataset is advised. Normal distribution is often set as a default assumption when normalizing/standardizing the dataset. Another area where normal distribution is positive is the distribution of the residuals. A normal distribution of these error terms can show that the errors are largely consistent across the dataset, or in other words, they are more or less equal for different the input values. The regression analysis with aforementioned reference values yields

$$log\,\mu^*(T^*, P^*, \dot{\gamma}^*) = 0.012 - 15.87\,log\,T^* + 0.032\,P^* + 0.060\,log\,\dot{\gamma}^* \tag{2}$$

Firstly, note that the $R^2 \approx 0.99$, and the standard errors are 0.002 for $log\,A$, 0.05 for a, 0.002 for b, and 0.002 for c. Low values indicate that the model is confident in the weighting of the coefficients. The VIFs of the predictor variables are found to be ≈ 1. This indicates that there is a low probability that there are any issues regarding multicollinearity. The last factor worth looking at is the distribution of residuals. For the logarithmic dataset, the residuals are distributed as displayed in Fig. 6. Evidently, the residuals are organized according to a normal distribution, with little negative skewness.

With $A = 1.01$, $a = -15.87$, $b = 0.032$, and $c = 0.060$, we get the power-law form as:

$$\mu^*(T^*, P^*, \dot{\gamma}^*) = 1.01\,{T^*}^{-15.87}\,e^{0.032P^*}\,{\dot{\gamma}^*}^{0.060} \tag{3}$$

Figure 7 shows the calculated viscosity, μ^*_{calc} using the above power-law against the measured, dimensionless viscosity from the experiment. An ideal plot would show a

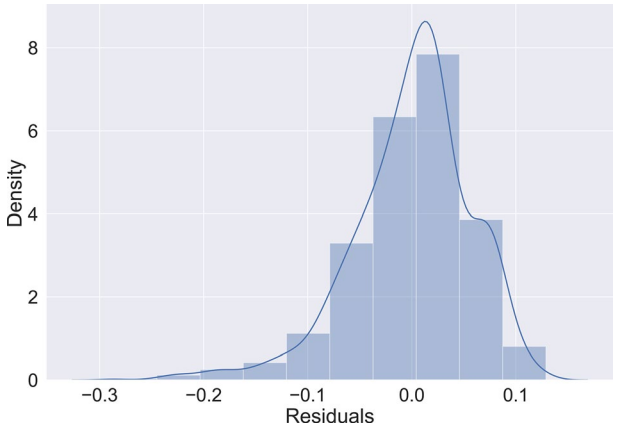

Fig. 6 Distribution of the residuals for the logarithmic dataset

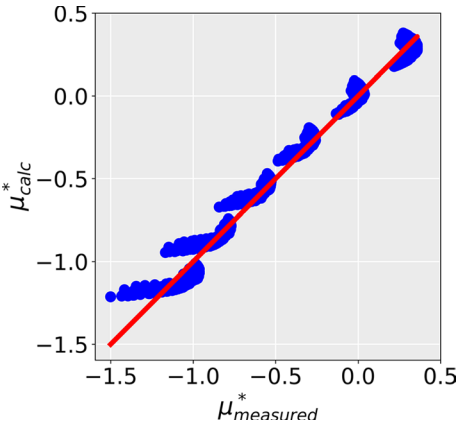

Fig. 7 Measured viscosity, $\mu^*_{measured}$ vs calculated viscosity, μ^*_{calc} from Eq. 3

Table 3 Reference states and their corresponding coefficients

	P (MPa)	T (K)	$\dot{\gamma}$ (s^{-1})	μ (mPa·s)
Ref1	0.1	273	300	105
Ref2	15	298	1000	28.9
Ref3	7.5	288	672	57.9
Ref4	7.5	278	452	77.6
Ref5	15	278	672	78.3
	A	a	b	c
Ref1	0.943	−15.87	0.0004	0.061
Ref2	0.978	−15.87	0.064	0.061
Ref3	0.793	−15.87	0.032	0.061
Ref4	1.01	−15.87	0.032	0.060
Ref5	1.06	−15.87	0.065	0.061

diagonal line perfectly, 1:1 ratio. The figure evidently shows that the power-law with the weighted coefficients is a good fit, placing itself along the diagonal red line.

The chosen reference state ultimately produces the coefficients for the fitted Equation 3. These coefficients vary based on the choice of the reference state. We summarize the set of different reference states and corresponding values of the fitting parameters in Table 3. The first two reference states (Ref1 and Ref2) are at two extremities, and the third state Ref3,is in the middle of the ranges (considering 300 s^{-1} as the lower bound of the shear rate). Ref4 is the one chosen for Equation 3, while Ref5 is at the targeted pressure of 15 MPa, targeted temperature, and the middle value of the shear rate.

We observe little or no variations of the parameters a and c. However, A and b vary with different choice of reference states. Note that the chosen reference state Ref4 yields the value of $A \approx 1$ and reproduces desired prediction of viscosity at the reference state.

In Table 1, several substances were shown together with the predictive model equation, as well as their coefficients, PVC values, and R^2 values. All the R^2 values present in that table lies between 0.988 and 1.000, and the model equations are based on either the Barus equation, or the Freitas equation. The present power-law does also resemble a Barus equation, and its R^2 value is close to the ones presented in Table 1, which again solidifies it as a good model for the scale inhibitor. Table 1 does also include different coefficients, η_0 values which corresponds to the term AT^a in Eq. 3. The η_0 values are problematic to compare with directly because the equations in Table 1 largely present η_0 as a function of temperature, meaning each η_0 value is fitted for a particular temperature. These equations are not fitted to the same material used in this experiment, so a direct comparison is not of much use. However, as an observation, the R^2 value of Equation 3 is promising for the fitting. Another interesting observation is the α values. In Table 1, these coefficients are listed in the column with PVC values. PVC is equal to α in the equations. The first 8 substances all are fitted to this equation: $\eta_P(T,P) = \eta_0(T)e^{\alpha(P-P_0)}$, where the α value is the PVC values in the 4th column. These are all in the range of 0.010 to 0.013, low values. The power-law derived in this paper has an α value, denoted as a, equal to 0.0324. Again, a direct comparison is not of much value given the different materials and equations. However, it is an interesting observation to make looking at these α values and that of Equation 3.

In a study by Bosco et al. [29] a mix of mainly polyethyleneglycol (PEG) and fumed silica particles were tested at atmospheric pressure and increasing shear rate, which showcased similar results as in this work. At low shear rates, a decrease is first seen, then an increase happens until a critical point. After this, the viscosity again decreases, acting like shear-thinning fluid. Even though PEG and MEG have highly different applications and fumed silica is used as a thickening agent, it's interesting to see the similarities between them as there has been found no other studies showing similar behavior. An explanation given by Bosco et. al regarding this behavior is that there is an inherent weakness of the geometry. This explanation correlates well with what has been described in Sect. 2.1 that these results are not logical. A possible explanation presented by Bosco et. al was that the surface-tension forces of the fluid are large enough to impede flow, contributing to this behavior. With all 20 wells part of the Tommeliten Alpha project in production, and all in need of maximum designed injection rate, the transport time for the fluid will be around 3 days. Maximum injection rate is rarely needed, at least not from the start, as not all wells will be active in the initiating phase of the project, and the scale inhibitor will be injected as the demand for it is there. Considering this, it can be assumed that the fluid can be in the pipeline and therefore under pressures of up to 170 bar for up to 4 weeks. Given that the scale inhibitor will be transported over a period of several weeks, it would be interesting to see if the chemical shows any thixotropic tendencies.

3.4 Limitations

The results presented have some limitations. Most of the literature review has been focused on work done up to 150 MPa. The test in this work was conducted up to 15 MPa, substantially lower than most of the literature. As these studies have shown a tendency for the viscosity to behave in an exponential way with regard to the increase of pressure for several different liquids, it can be reasonable to assume that the chemical tested in this work would behave the same way. However, as the instrument used was restricted to a maximum of 15 MPa, and the request from Aker Solutions was to test the liquid up to this pressure, this assumption remains uncertain in large. Another point to be made is that the pressure range tested in 0.1–15 MPa is, for most of the studies reviewed, in an area where the piezoviscous effects still remain quite negligible. To see if this exponential behavior exists for this chemical, further experiments must be conducted at higher pressures. The existing operating conditions for this liquid is, however, not subjected to higher pressures than what has been tested. For the data looking at how the viscosity changes with shear rate, it is important to note that for shear rates around 100–300 s^{-1} , there exist many data points. Above this limit, the number of data points is lower for each hundred s^{-1}. This makes the results at higher shear rates prone for uncertainties.

Truly understanding this liquid is of great difficulty as the deformation history is unknown. The manufacturer's secrecy regarding the contents makes it difficult to accurately draw conclusions and find similarities with existing literature and existing models. An aspect that can affect viscosity of a liquid is thixotropic behavior, time dependency of viscosity. To understand this, one would need to know how the liquid has been treated prior to the experiment. Has it been subjected to any elevated pressures, temperatures or shear rates? In almost all cases, these history parameters are unknown, reducing the validity of any discussion of thixotropy. A major limitation for this work is the lack of an exact chemical composition of the scale inhibitor, and that it was not allowed to test the substance for its physical and chemical properties. By having these restrictions, it limits the ability to delve into the molecular structure-aspect. The molecular shape of the substance could provide more information and possibly help the creation of other predictive models.

4 Conclusions

In this work, an experiment looking at how the viscosity of a scale inhibitor used in the oil & gas industry varies with increasing pressures from atmospheric pressure to 15 MPa has been conducted. A systematic review of the existing literature has been performed. Most of the literature reviewed reported viscosity changes due to pressures up to 150 MPa, substantially higher than this work. This leaves openings for future experimentation, especially at higher pressures. Given the concerns brought to light by both Bosco et. al and professionals at IFE, the steep increase in viscosity at low shear rates is, by the group, discarded as being a victim to a weakness of the geometry. Considering the miniscule changes of viscosity with pressure and shear rate,the scale inhibitor studied in this work exhibits near Newtonian behavior. The

power-law fitted for this experiment does show promising R^2 values, close to those of Table 1, as well as an α, or a value, similar to that found in the literature. The plot showing calculated viscosity versus measured viscosity displays a cluster of points following the diagonal line closely, meaning the power-law model is a good fit. As noted in the introduction, results showing no changes in viscosity due to pressure and shear rate are optimal. This work verifies that the rheological properties of the scale inhibitor in question are ideal for its purpose.

Acknowledgments This work is an extract from the Bachelor thesis project work of first three authors performed during the spring semester of 2022 at the Department of Civil Engineering and Energy Technology, Oslo Metropolitan University. The authors greatly acknowledge the support from Leif Inge Wiig of Aker Solutions, and Serkan Keleşoğlu of Institute for Energy Technology (IFE), Norway.

Author contribution Conceptualization, formal analysis, investigation, SKG, EFS, ESE; writing–original draft preparation, SKG, EFS, ESE and AC; writing–review and editing, SKG, AC and HBM; supervision, AC; project administration, AC All authors reviewed the manuscript.

Funding Open access funding provided by OsloMet - Oslo Metropolitan University. Not applicable.

Data availability The data presented in this study are available on request from the corresponding author.

Declarations

Competing interests The authors declare no competing interests.

Ethical approval Not applicable.

References

1. M. Crabtree, D. Eslinger, P. Fletcher, M. Miller, A. Johnson, G. King, Fighting scale: removal and prevention. Oilfield review **11**(03), 30–45 (1999)
2. H. Wigg, M. Fletch, Establishing the True Cost of Downhole Scale Control. Conference// International Conference on Solving Oilfield Scaling. - Aberdeen, Scotland (1995)
3. O.E. Agwu, J.U. Akpabio, M.E. Ekpenyong, U.G. Inyang, D.E. Asuquo, I.J. Eyoh, O.S. Adeoye, A comprehensive review of laboratory, field and modelling studies on drilling mud rheology in high temperature high pressure (hthp) conditions. J. Nat. Gas Sci. Eng. **94** (2021)
4. J.G. Lenard, *Primer on Flatrolling*, 2nd edn, (Elsevier, Amsterdam, 2014), pp. 193–266
5. K.O. Geddes, S.R. Czapor, G. Labahn, *Algorithms for Computer Algebra* (Kluwer, Boston, 1992)
6. S.C. Vant, Investigation of fluid properties at non-ambient conditions. PhD thesis, University of Strathclyde (2003)
7. R.L. Cook, C.A. Herbst, H.E. King Jr, High-pressure viscosity of glass-forming liquids measured by the centrifugal force diamond anvil cell viscometer. J. Phys. Chem. **97** (1993)

8. A. Ahuja, R. Lee, Y.M. Joshi, Advances and challenges in the high-pressure rheology of complex fluids. Adv. Colloid Interface Sci. **294** (2021)
9. J.M.L. del Río, M.J. Guimarey, M.J. Comunas, J. Fernandez, High pressure viscosity behaviour of tris (2-ethylhexyl) trimellitate up to 150 mpa. J. Chem. Thermodyn. **138**, 159–166 (2019)
10. M. Sobrino, E.I. Concepcion, A. Gomez-Hernandes, M.C. Martin, Viscosity and density measurements of aqueous amines at high pressures: Mdea-water and mea-water mixtures for co2-capture. J. Chem. Thermodyn. **98**, 231–241 (2016)
11. S.V.D. Freitas, J.J. Segovia, M.C. Martín, J. Zambrano, M.B. Oliveira, M.B. Limax, J.A.P. Coutinho, Measurement and prediction of high pressure viscosities of biodiesel fuels. Fuel **122**, 223–228 (2014)
12. T.G. Mezger, *The Rheology Handbook*, 4th edn (Vincentz Network, 2014)
13. C. Barus, Isothermals, isopiestics and isometrics relative to viscosity. Am. J. Sci. 3–45 (1893)
14. A.G.M. Ferreira, N.M.C. Talvera-Prieto, A.A. Portugal, R.J. Moreira: Review: models for predicting viscosities of biodiesel fuels over extended ranges of temperature and pressure. Fuel **287** (2021)
15. D. Tomida, A. Kumagai, K. Qiao, C. Yokoyama, Viscosity of [bmim][pf6] and [bmim][bf4] at high pressure. Int. J. Thermophys. **1**(27), 39–47 (2006)
16. A.M. Duncan, A. Azita, R. McHenry, C.D. Depcik, S.M. StaggWilliams, A.M. Scurto, High-pressure viscosity of biodiesel from soybean, canola, and coconut oils. Energy Fuels **24**, 5708–5016 (2010)
17. C.J. Schaschke, S. Allio, E. Holmberg, Viscosity measurement of vegetable oil at high pressure. Food Bioprod. Process. **84**, 173–178 (2006)
18. C.J. Schaschke, J.M. Paton, Viscosity measurement of biodiesel at high pressure with a falling sinker viscometer. Chem. Eng. Res. Design **87**, 1520–1526 (2009)
19. A. Cameron, *The Principles of Lubrication*, 1st edn. (Wiley, New York, 1966)
20. A.Z. Szeri, *Fluid Film Lubrication*, 1st edn. (Cambridge University Press, Cambridge, 1998)
21. G.W. Stachowiak, A.W. Batchelor, *Engineering Tribology*, 4th edn. (Elsevier, Oxford, 2016)
22. B.J. Hamrock, S.R. Schmid, B. Jacobson, *Fundamentals of Fluid Film Lubrication*, 2nd edn. (Marcel Dekker, Inc, 2004), p. 115
23. R.P. Chhabra, J.F. Richardson, *Non-Newtonian Flow and Applied Rheology*, 2nd edn., (Butterworth Heinemann, 2008), pp. 9–55
24. S. Mortazavi-Manesh, J.M. Shaw, Effect of pressure on the rheological properties of maya crude oil. Energy Fuels **30**, 759–765 (2016)
25. J. Hermoso, F. Martinez-Boza, C. Gallegos: Influence of viscosity modifier nature and concentration on the viscous flow behaviour of oil-based drilling fluids ad high pressure. Appl. Clay Sci. **87** (2014)
26. J. Chaoa, L. Zhang, R. Feng, Z. Wang, S. Xu, C. Zhang, S. Ren: Experimental study on the compatibility of scale inhibitors with mono ethylene glycol. Product. Chem. **5** (2020)
27. S. Budavari, *The Merck index*, 11 edn. (Merck & CO, Inc., 1989), p. 599
28. Anton Paar GmbH: DG geometry. Anton Paar, Doube gap gemotry (2020). https://www.anton-paar.com/?eID=documentsDownload&document=18378&L=0
29. A. Bosco, V. Carado, J. Maia Rheological parameters of shear-thickening fluids using an experimental design. Mater. Res. **1** (2018)